# Cathodic delamination kinetics of thin polystyrene model coatings bound to zinc via organosilanes

Danish Iqbal, Julian Rechmann, Asif Bashir, Adnan Sarfraz, Abdulrahman Altin, Andreas Erbe*

*Danish Iqbal, Julian Rechmann, Asif Bashir, Adnan Sarfraz, Abdulrahman Altin*
Max-Planck-Institut für Eisenforschung GmbH, 40237 Düsseldorf, Germany

*Andreas Erbe*
Max-Planck-Institut für Eisenforschung GmbH, 40237 Düsseldorf, Germany
Department of Materials Science and Engineering, NTNU, Norwegian University of Science and Technology, 7491 Trondheim, Norway
E-Mail: PS-delamination-zinc@the-passivists.org

The cathodic delamination of poly(styrene) [PS] model coatings from oxide-covered zinc has been evaluated by scanning Kelvin probe (SKP). Linear and acrylate cross-linked PS model coatings covalently bound to zinc oxide via Zn-O-Si bonds have been prepared. PS was prepared by thermally initiated free radical polymerization in the presence of vinyltrimethoxy silane modified zinc. Cross-linkers ethylene glycol diacrylate (EDA) and hexanediol diacrylate (HDA) were used in some preparations. Resulting polymers are 8-15 nm thick. PS model coatings show a delamination rate of only ≈20% of that of comparable poly(methyl methacrylate) [PMMA] samples. The slower cathodic delamination of PS is attributed to denser chain packing and higher amounts of hydrophobic moieties, leading to a reduction in penetration of corrosive species. As opposed to the situation in PMMA, the addition of HDA

increases the delamination rate, due to its flexible chains and hydrophilic groups. The lowest delamination rate is observed in the presence of 25% EDA. Consequently, ester hydrolysis of acrylates accelerates delamination, it is however not the main factor in cathodic delamination of such thin model system.

Keywords: cathodic disbonding; crosslinking; grafting density; interface chemistry; organic coating; packing; polymer coating; poly(styrene); scanning Kelvin probe

# 1 Introduction

Organic coatings used in corrosion protection on metals may fail due to chemical decomposition, anodic undercutting or cathodic delamination.[1, 2] The latter process is particularly fast under humid conditions on materials with a low-band gap oxide, such as steels and galvanized steels.[2, 3] The progress of the position $d$ of a delamination front with time $t$ during cathodic delamination is usually described by a power law with exponent $\alpha$ in the form of $d \propto t^{\alpha}$. Traditionally, $\alpha = 1/2$ has been observed in many cases and attributed to a diffusion controlled process.[4–6] Furthermore, $\alpha = 1$ is sometimes observed, and attributed to reaction control by a first order chemical reaction,[7] or short-distance ion migration,[8] as rate controlling steps. Especially ion mobility can also be assessed at insulator surfaces, permitting separation of different reactions.[9] More recently, self-healing coatings were realised with $\alpha \to 0$ after certain times, due to a slow-down in cathodic delamination rate.[10–14] In addition, cross over between different exponents has been observed.[15, 16] For applications, both the characteristic exponent $\alpha$ as well as the delamination rate $r$, defined here as time derivative of the progress of the delamination front, $r = \mathrm{d}d/\mathrm{d}t$, shall be as low as possible. To further the academic understanding of what governs both quantities on the molecular level, the study of defined model systems may be a fruitful approach.

Adhesion strength at polymer/metal interface is vital in defining the corrosion protection

properties of a polymer coating,[5, 17] hence also is crucial for both the delamination rate and $\alpha$ in a certain process. The barrier properties of polymer coating against species like oxygen and water also play a vital role in defining the final corrosion protection performance of an organic coating.[2] The permeability of these species through the coating is determined by the structure and morphology of the protective organic film.[18] The tranport of gases such as oxygen or nitrogen is governed by a diffusion process present in the polymer, as these species hardly interact with the polymer. Therefore, the structural attributes such as holes and defects in a polymer structure can significantly increase the transport of oxygen through the coating. On the other hand, permeability of water is strongly governed by the solubility due to strong interaction with the polymer.[18] It has been shown that the presence of water and oxygen are essential for initiation of a corrosion reaction. Water is essential to establish an electrochemical corrosion cell beneath the coating and oxygen reduction is often the central cathodic counterreaction to the corrosion process.[18, 19]

Polymer structural attributes are important in corrosion protection. In particular, close packing of polymer chains and higher fractions of hydrophobic groups lead to enhanced resistance against permeation of water and oxygen.[20] Moreover, it has been shown that polymers containing stiff monomers such as aromatic rings tend to significantly reduce the diffusion of water molecules through the polymer chains.[21]

In a previous work from our group, the cathodic delamination has been studied of covalently surface-bound linear and cross-linked poly(methyl methacrylate) [PMMA] model coatings.[7] Containing an ester bond along the main chain such as in an acrylate makes the polymer prone to alkaline hydrolysis of the ester. In addition, PMMA has a higher chain flexibility when compared to aromatic polymers such as poly(styrene) [PS]. Because aromatic polymers exhibit enhanced barrier properties against water and oxygen compared to aliphatic polymers, it is expected that they also show enhanced resistance against cathodic delamination.[18]

Hence, the aim of this work is to study the cathodic delamination of PS polymers, linked

via siloxanes to oxide-covered zinc. Moreover, cross-linked PS coatings were synthesized by addition of aliphatic bifunctional molecules during the polymerization reaction. The overall approach in this work closely follows the approach persued in ref. [7].

# 2 Experimental section

## 2.1 Materials

Zinc sheets with a thickness of 1.5 mm and purity of 99.95% were obtained from Goodfellow (Cambridge, UK). Vinyltrimethoxy silane (VTS), ethylene glycole diacrylate (EDA), hexanediol diacrylate (HDA), styrene, azobisisobutyronitrile (AIBN), toluene and ethanol were purchased from Sigma-Aldrich (Steinheim, Germany). AIBN was recrystallized in ethanol prior to use. All other chemicals were used as received. Zinc substrates (15 mm $\times$ 15 mm) were initially mechanically ground with SiC paper up to 4000 grit, followed by polishing with silicon paste of 1 µm to have a smooth surface, in order to exclude effects of morphology, as discussed elsewhere.[22] After polishing, the substrates were first thoroughly washed with deionized water followed by cleaning with ethanol in an ultrasonic bath and dried under a dry stream of nitrogen. All synthesis steps were performed under inert atmosphere in standard Schlenk tubes.

## 2.2 Surface modification

The overall synthesis strategy for the growth of linear and cross-linked PS coatings is illustrated schematically in Figure 1. Initially polished zinc samples were immersed in 0.1 M NaOH for 1 min to increase the concentration of hydroxyl groups.[23] Afterwards, zinc surfaces were treated with VTS to obtain a vinyl-terminated, silane modified zinc substrate by a silanization reaction.[24] The functionalization reaction was carried out at room temperature by immersion of a polished zinc substrate in an ethanol/water mixture (90:10) containing 1 mL (0.007 mmol) of VTS. After one day, the sample was removed, cleaned sequentially with

excess acetone and ethanol to remove physisorbed molecules, and dried under a pressurized nitrogen stream.

Before polymerization reactions, toluene (40 mL) was degassed by performing three freeze-thaw-pump cycles. Subsequently, 1 mL styrene (0.01 mol) and 0.003 g AIBN (0.3 wt% relative to styrene) were added under stirring. A functionalized zinc sample was then introduced into the reaction mixture and the temperature was raised to 70°C in order to initiate a polymerization reaction. After 24 h the zinc sample was removed, washed with excess acetone, followed by ultrasonic cleaning for 1 min in toluene in order to remove any remaining traces of physisorbed polymer. Finally, samples were dried in a dry stream of nitrogen.

Cross-linked polymer coatings were synthesized on modified zinc substrates by the same polymerization procedure, except additional crosslinking agent (EDA or HDA) with different molar fractions (25% or 50%) was added to the solution. The total monomer concentration (EDA/HDA + styrene) was kept constant.

## 2.3 Characterization methods

The modified zinc samples were characterized by infrared (IR) spectroscopy on a Bruker Vertex 70v Fourier transform IR spectrometer. IR spectra were taken in external reflection geometry with a spectral resolution of 4 $cm^{-1}$ at an angle of incidence of 80° using p-polarized light.[25] A liquid nitrogen cooled, middle band mercury cadmium telluride detector was used for detection. Prior to surface modification, background spectra were obtained from freshly pretreated zinc samples. The reflectance absorbance spectra shown in this work were recorded against these backgrounds.

X-ray photoelectron spectroscopy (XPS; Quantum 2000, Physical Electronics) was used to analyze the chemical composition of the functionalized and polymerized sample surfaces. XPS measurements were performed at a take-off angle of 45°, with a monochromatic Al K$\alpha$ source (1486.6 eV). The 1s elemental peak from carbon (285 eV) and 2p from silicon (103 eV) were measured with high resolution (energy step 0.2 eV, pass energy 22.5 eV).

The thickness of the polymer coatings was determined by performing ellipsometry measurements using a UV/visible spectroscopic ellipsometer (SE 800; Sentech Instruments) in the wavelength range of 400-800 nm. Measurements at three spots per sample were taken with an incident angle of 70°. Differences in ellipsometric parameters with respect to the bare zinc substrate were analyzed. Film thickness of the polymer layers on samples, regardless of modification, was obtained by fixing the refractive index of the organic part coatings to 1.5, and considering it in first approximation as wavelength-independent. The value of 1.5 is generic for an organic substance and not far from the refractive index of PS of 1.59.[26]

## 2.4 Evaluation of electrochemical stability

Cathodic delamination experiments were performed on a commercial scanning Kelvin probe (SKP) system from KM Soft Control (Wicinski - Wicinski GbR, Wuppertal, Germany) with a 100 µm NiCr tip in humid air and nitrogen atmospheres. Before each experiment, the Kelvin probe was calibrated to the standard hydrogen electrode (SHE) against a $Cu/CuSO_4$ reference electrode. The potential of the intact polymer coating measured at the beginning was used to correct for drifts during the experiments. Details of the SKP's working principle have been described elsewhere.[27]

Zinc samples with thin PS coatings produced here were spin coated with 5 wt% poly(vinyl butyral) [PVB] in ethanol to yield a 1 µm thick polymer film. This PVB coating prevents the spreading of the electrolyte on the PS-coated zinc samples. Unmodified zinc substrates were spin coated with PVB and cathodic delamination experiments were performed under similar conditions to evaluate the effect of PVB alone.

In order to initiate a cathodic delamination process, an artificial defect was created at the edge of the sample with a scalpel, and the defect was filled with 1M KCl. The samples were subsequently introduced into a humid SKP chamber at 92-95% relative humidity at a temperature around 23 °C. The progress of the delamination front was analyzed as described elsewhere.[28] As position of the delamination front, the first point which shows the potential

of the intact interface was used. Typically, 3 to 5 samples for each given preparation were analyzed. The results presented are results of the median sample, i.e. after sorting the samples in the order of increasing stability, the sample with the middle performance was selected for comparative analysis of delamination rates. Representations of the full datasets are not shown to keep graphs legible.

Linear polarization experiments were performed by using a Voltalab Radiometer PST050 potentiostat in 0.1 M KCl electrolyte at a scan rate of 5 mV/s. The potentiodynamic measurements were started after 1 h stabilization time of the open circuit potential (OCP) from +100 mV vs. OCP anodic to -200 mV to the cathodic direction. The samples analyzed had an area of 0.63 $cm^2$. All experiments were performed in a self-made 3 electrode setup, where a graphite rod was used as counter electrode. A commercial Ag/AgCl/3M KCl reference electrode (Metrohm) served as reference electrode. All potentials are quoted here versus standard hydrogen electrode (SHE).

The corrosion current densities $i_{\mathrm{corr}}$ were calculated from the polarization resistance $R_{\mathrm{p}}$ according to an established procedure.[29] $R_{\mathrm{p}}$ was determined as the slope of the linear polarization curve from -15 mV to +15 mV around the corrosion potential $E_{\mathrm{corr}}$. The Tafel slopes of the anodic and cathodic branch,$\beta_{\mathrm{a}}$ and $\beta_{\mathrm{c}}$, respectively, were obtained from linear regions of the Tafel plots. Corrosion current densities were then calculated as [29]

$$i_{\mathrm{corr}} = \frac{\beta_{\mathrm{a}}\beta_{\mathrm{c}}}{\ln(10)R_{\mathrm{p}}(\beta_{\mathrm{a}} + \beta_{\mathrm{c}})}. \quad (1)$$

# 3 Results and Discussion

## 3.1 Synthesis and Characterization of PS-coated zinc

Schematically, the preparation is shown in Figure 1. The modification of zinc substrate with VTS and characterization with IR, XPS and TOF-SIMS were carried out in close analogy to the synthetic route used for PMMA.[7] In particular, the first step of the procedure, the

modification of zinc with VTS was identical, and shall hence not be discussed again in this work. Importantly, Zn-O-Si bonds were formed, as demonstrated previously by the presence of the $ZnOSi^+$ fragment in time of flight secondary ion mass spectrometry (Fig. 1c in ref. [7]). The presence of the $ZnOSi^+$ fragment is an indication of the formation of a covalent bond between organosilane and the native oxide on zinc.[30] IR spectroscopy (Figure 2a) shows characteristic peaks of hydrocarbons and organosilanes.[31, 32] XPS (Figure 2b) shows the Si 2p peak expected on the surface after modification with VTS. A detailed discussion of these spectra is available elsewhere.[7]

After successful functionalization of zinc surface with VTS, PS was grown on top of functionalized zinc surface via thermally initiated free radical polymerization of styrene in the presence of AIBN as a thermal initiator (Figure 1). As in the case of free radical polymerization of MMA,[7] two fractions of PS polymer were formed. One fraction was covalently bonded to the substrate, incorporating surface-bound monomers, while the other fraction was either physisorbed on the surface or present in the solvent phase. The physisorbed polymer was removed by cleaning with acetone and toluene.

In addition to linear PS polymer, cross-linked PS coatings were synthesized on top of functionalized zinc samples by adding a bifunctional cross-linking molecule at the start of polymerization reaction that leads to cross-linked polymer coatings. The bifunctional molecules used were of different chain lengths (ethyl and hexyl) and were added in different molar ratios (25 mol% and 50 mol%) to yield polymer coatings with different cross-linking densities.

The prepared polymer model coatings were characterised by IR spectroscopy (Figure 3, Table 1) and the C 1s region in XPS (Figure 4). The IR bands at 1589 and 1494 $cm^{-1}$ are assigned to the aromatic ring stretching modes from the benzene rings in the PS polymer.[31] The band present at $\approx$3060 $cm^{-1}$ is assigned to the C-H stretching mode of aromatic rings.[31] The presence of the signals of the aromatic ring confirms the successful growth of PS polymer coating on top of the silane modified zinc substrate. In case of cross-linked coatings, the presence of C=O stretching mode at around 1725 $cm^{-1}$ confirms the presence of ester

functionality that comes from the cross-linking moiety.

Figure 4 shows the high resolution C 1s XP spectra of covalently bound PS model coatings on zinc. Each peak was fitted with four components. The main component centered at 284.8 eV arises from the polymer's C-C and C-H bonds. C-O bound carbon atoms and the respective neighbouring C atoms show up as shoulder at higher binding energies and are centred around 286.4 and 285.4 eV, respectively. The peak at 288.8 eV arises from C=O carbon present in the acrylate based cross-linkers in the polymer coating. The presence of the C=O component in the non-crosslinked, pure PS (Figure 4a) is unexpected, but in agreement with the presence of a C=O stretching mode in the respective IR spectrum. The adsorption of atmospheric contaminants leads usually to different peaks with significantly less C=O. An analysis of the IR spectrum of the non-surface bound polymer which formed in solution (not shown) does not exhibit the characteristic C=O stretching mode at 1730 $cm^{-1}$. Therefore, we do not treat this component in more detail. Its presence can only be explained by slight oxidation of some components.

The thicknesses of the as synthesized polymer coatings as determined by ellipsometry are summarized in Table 2. Compared to the work with PMMA, thicknesses show the same behaviour with cross-linkers as for PMMA.[7] The more cross-linking agent is added, the more dense the polymer film gets and the thinner is the resulting layer.

## 3.2 Stability against cathodic delamination

SKP measurements were used to evaluate the stability of the synthesised model coatings against cathodic delamination. To avoid spreading of 1M KCl over the surface, the samples were covered with an ≈1 µm thick PVB film by spin coating. PVB also served the purpose to level out differences in thickness which would affect the diffusion of species to the interface. SKP experiments were performed under similar experimental conditions as carried out for chemisorbed PMMA coatings.[7]

Figure 5 shows the SKP potential profiles for selected investigated samples. In addtion,

results of a control experiment with spin coated PVB is also shown. The curves show the typical shape and progression through the experiments.[10, 28] Initially, the potential of the intact polymer/metal interface, ≈0.0 to 0.2 V, is obtained. With time, the region is increasing in which the potential of corroding zinc, ≈-0.5 to -0.7 V, is observed. Both potential levels are separated by a transition region. (Slight potential changes with time on both the passive side and the corroding side have been observed, but may e.g. be due to charging induced drift. Therefore, these effects shall not be discussed here.) In the case of PVB, immediately after the transition region from the region of the intact polymer, there is a narrow region in which the potential decreases to a level below the steady state potential of the corroding zinc in the defect. We attribute this "overshoot" as a sign of the spatiotemporal pattern formation which has been observed for this system, with osciallations in pH, water content and ZnO amount.[33, 34] Under the experimental conditions used here, the oscillations observed previously are not as clearly visible. In the experiments with the different PS-based model coatings, this overshoot is absent. The transition region is not as sharp as observed for pure PVB. This difference may be related to the longer duration of experiments, such that diffusion processes during delamination may spread the delamination front.

Interestingly, in many experiments with samples from the PS series, an increase by ≈0.1 V of the potential at the non-delaminated side is observed before the transition region where the delamination front is located. As this increased potential is in the same region relative to the transition region all the time it is not due to a measurement artifact. This increase could indicate an increased passivation before the actual delamination process occurs. For example, water reaching the interface may increase the cross-linking of the Si-O network by hydrolysis of remaining Si-$OCH_3$ groups, hence ensuring the presence of a denser siloxane layer. The interpretation that water is playing a role here is in line with the observation in previous work of water vibrational modes in in situ Raman and IR experiments before the major part of the delamination process occurrs.[33, 34] However, for pure PVB such increase was not observed, and hence is likely not caused e.g. by oxidation of zinc or other processes

which could also happen in PVB. A Donnan potential is also unlikely to affect the region of the intact polymer.

The delamination rates were calculated from linear fits to the initial linear regions of the progress in cathodic delamination front with time (Figure 6a) and are included in Table 2. The same results were plotted on a double logarithmic scale (see Figure 6b) which enables to determine the exponent $\alpha$ of the time dependence. The double logarithmic plot shows that initially, $\alpha \approx 1$ for all experiments, justifying the determination of a delamination rate by a simple linear fit. With time, $\alpha$ decreases for some samples. These results indicate that delamination rates are not diffusion controlled at least in the initial part of the experiment. It is evident from Figure 6 and Table 2 that pure PVB with $r \approx 11.0 \pm 0.05$ mm $h^{-1}$ has an >20 times higher delamination rate than all the other systems in this study.

## 3.3 Electrochemical properties

Linear polarization experiments are another means of assessing corrosion resistance of different surfaces. Tafel plots for bare and coated zinc surfaces are shown in Figure 7. As opposed to the SKP experiments, no PVB top coating was present on top of the PS model coatings in those experiments. Corresponding corrosion current densities were calculated according to Equation (1). Tafel slopes, polarization resistance and corrosion current density for each system are summarised in Table 3. Corrosion rate is the highest for non-coated zinc, reflected in high corrosion current density.

## 3.4 Discussion and comparison

Similar to the observations for thin PMMA-based model coatings,[7] the covalently bound systems show significantly reduced cathodic delamination rates compared to the pure PVB reference. At approximately half the thickness, non-crosslinked PS with the same interface linkage as PMMA delaminated with a delamination rate of 1/5 of that of PMMA. Obviously, the chain packing in PS makes PS more protective than PMMA. Aromatic PS is also

more hydrophobic than PMMA, which likely contributes to the lower delamination rate.[35] However, there is not much difference in the delamination rates for cross-linked PS coatings, which is different from the situation for PMMA.[7] The possible explanation for this observation is that addition of aliphatic cross-linking molecules effects the close packing of aromatic rings and increases the hydrophilicity of polymer chains due to presence of polar carboxylate groups in a cross-linking molecule. Hence, there is not a significant decrease in the delamination rates for cross-linked PS coatings. This interpretation is supported by comparing the delamination rates of PS coatings with different molar ratios of EDA and HDA. Rates listed in Table 2 show that the addition of higher amounts of cross-linker leads to an increase in the delamination rates of PS coatings, as the fraction of acrylate is increased. Moreover, a cross-linker with longer aliphatic chain also increases the delamination rate. This effect can be again explained by the morphology and structure of the polymer chains. Higher amounts of aliphatic cross-linker disturb the close packing of the aromatic moieties and hence, more free volume is present in the polymer chain structure. Similarly, the cross-linker with a longer aliphatic chain in HDA destroys the close polymer chain packing due to higher chain mobility. Interestingly, the trend with addition of crosslinker is opposite to the trend observed for PMMA.[7] While in PMMA, the same crosslinking increased stability, in PS the introduction of acrylate decreases interfacial stability.

Looking at the results from the LPR experiments (Table 3) shows that obviously, covering zinc with noncrosslinked PS via a covalent bond significantly reduces the corrosion current density, as the organic polymer separates the reactive surface from the corrosive environment. Before proceeding to a discussion of the $i_{\mathrm{corr}}$, it is worth noting the differences in anodic Tafel slopes between the different samples, which is not supposed to exist, and which also does not follow any trend. This difference may stem from the intrinsic limitation of the LPR experiment,[36] in which one needs to polarise over quite a significant potential range (here 100 mV) in order to determine the Tafel slopes. The surface damage following from this polarisation may be different from sample to sample and may be the reason for the observed

differences with no obvious trend.

Comparing $i_{\mathrm{corr}}$ as before between non-crosslinked PS and PMMA[7] mirrors the trend observed in the delamination rates: $i_{\mathrm{corr}}$ of the PS model coating is $\approx 1/20$ of that of comparable PMMA samples. In the series on PS in this work, a distinct effect of cross-linking agents was observed in the values of $i_{\mathrm{corr}}$. While the flowing current is further depressed by adding cross-linker with shorter chains, presumably due to a generation of denser polymer layers, addition of HDA with its longer aliphatic backbone led to increased $i_{\mathrm{corr}}$ compared to non-crosslinked PS. These observations support the interpretations of SKP experiments, as long-chain molecules disturb the ordering and packing density of the aromatic rings, leading to free volume for water and oxygen to penetrate through the polymer. EDA, however, increases up to a certain amount the structuring of the polymer and thus the protective barrier properties against corrosion. Overall, PS forms a denser film than PMMA, which is attributed here due to interactions between the aromatic ring systems, leading to lower reaction rates and an increase in polarization resistance.

An important difference between PS and PMMA is that PMMA may hydrolyse to hydrophilic and soluble polyacrylic acid, which is supposed to increase the the accessibility of water at the polymer/metal interface. The absence of this mode of degradation may also contribute the slower degradation in the PS system. However, introduction of 25% EDA into PS leads to a decrease in both delamination rate and corrosion current density, while at the same time it introduces carboxylate groups which could be hydrolysed. Therefore, alkaline hydrolysis of an acrylate cannot be the main factor leading to cathodic delamination of such acrylate-containing model systems.

In the corrosion literature in general, delamination rate $d$, corrosion current density $i_{\mathrm{corr}}$ and polarisation resistance $R_{\mathrm{p}}$ are all linked to interfacial stability. It is therefore instructive to plot these parameters against each other to evaluate to which extend one can substitute the other. A plot of $i_{\mathrm{corr}}$ and $R_{\mathrm{p}}$ versus $d$ is shown in Figure 8. (Plotting $i_{\mathrm{corr}}$ versus $R_{\mathrm{p}}$ is less useful, as $i_{\mathrm{corr}}$ is calculated from $R_{\mathrm{p}}$.) The expectation is that a system with low $d$

shows a large $R_p$ and a low $i_{corr}$. For the PMMA system (Figure 8b), this expectation is qualitatively fulfiled. For the PS system from this work, however, this correlation is only partly observed. It is therefore not obvious that one of the quantities alone can be used to characterise sufficiently the electrochemical degradation of the system. One reason may be the fact that coating inhomogeniety contributes in different fashions to results of cathodic delamination measurements and linear polarisation experiments. The latter should show the absence charge transfer for a pore-free coating. However, such thin systems as investigated here will likely have some pores. $R_p$ may thus in first approximation be seen as sampling the imperfections in the model coatings, while the delamination rate samples the average system performance. Unfortunately, for this particular system, the observed lateral inhomogeniety of the films themselves prohibits a quantitative evaluation of the pores, such as size and density.

# 4 Summary and conclusions

Cathodic delamination kinetics and electrochemical properties have been investigated of linear and cross-linked PS coatings that are covalently linked to zinc via organosilanes. These ultrathin coatings were synthesized on top of a zinc substrate via thermally initiated free radical polymerization of styrene. The results show that the covalently surface bound PS coatings exhibit only 0.4% of the delamination rate of a weakly bound PVB coating, which was also present on top of the other model coatings. Addition of aliphatic cross-linking agents does not lead to a significant reduction in the cathodic delamination rates. In particular, PS coatings cross-linked with EDA exhibit slower delamination rates than the coatings cross-linked with HDA. The addition of the HDA cross-linker with its hexyl chain affects the packing of aromatic groups that are present in the PS polymer and hence, leads to lower resistance against cathodic delamination.

*Acknowledgements*

D.I. acknowledges a scholarship from the IMPRS Surmat. A.S. acknowledges support from the Max Planck Society via Maxnet Energy. A.A. and A.E. acknowledge the DFG (Deutsche Forschungsgemeinschaft) for the financial support of the subproject ER 601/3-1 within priority program 1640 "Joining by plastic deformation". This work is supported by the Cluster of Excellence RESOLV (No. EXC 1069) funded by the Deutsche Forschungsgemeinschaft within the framework of the German Excellence Initiative.

# 5 References

1. O. Ø. Knudsen, A. Forsgren, *Corrosion Control Through Organic Coatings, Second Edition*, CRC Press, Boca Rayton, USA **2017**.

2. G. Grundmeier, A. Simões, in A. Bard, M. Stratmann, G. Frankel (Eds.), *Encyclopedia of Electrochemistry*, vol. 4, Wiley-VCH, Weinheim, Germany, chap. 5.4 - Corrosion Protection by Organic Coatings **2007**, 500–566.

3. C. D. Fernández-Solis, A. Vimalanandan, A. Altin, J. S. Mondragón-Ochoa, K. Kreth, P. Keil, A. Erbe, in R. P. Lang, Y. Liu (Eds.), *Soft Matter at Aqueous Interfaces, Lect. Notes Phys.*, vol. 917, Springer, Cham, Switzerland, chap. 2 - Fundamentals of Electrochemistry, Corrosion and Corrosion Protection **2016**, 29–70.

4. A. Leng, H. Streckel, M. Stratmann, *Corros. Sci.* **1998**, *41*, 579.

5. R. Posner, M. Santa, G. Grundmeier, *J. Electrochem. Soc.* **2011**, *158*, C29.

6. N. Wint, S. Geary, H. N. McMurray, G. Williams, A. C. A. de Vooys, *J. Electrochem. Soc.* **2015**, *162*, C775.

7. D. Iqbal, J. Rechmann, A. Sarfraz, A. Altin, G. Genchev, A. Erbe, *ACS Appl. Mater. Interfaces* **2014**, *6*, 18112.

8. R. Montoya, F. García-Galván, A. Jiménez-Morales, J. Galván, *Corros. Sci.* **2014**, *82*, 432.

9. M. Rohwerder, S. Isik-Uppenkamp, M. Stratmann, *Electrochim. Acta* **2009**, *54*, 6058 .

10. C. Glover, C. Richards, G. Williams, H. McMurray, *Corros. Sci.* **2018**, *136*, 304 .

11. A. Altin, M. Rohwerder, A. Erbe, *J. Electrochem. Soc.* **2017**, *164*, C128.

12. T. H. Tran, A. Vimalanandan, G. Genchev, J. Fickert, K. Landfester, D. Crespy, M. Rohwerder, *Adv. Mater.* **2015**, *27*, 3825.

13. A. Vimalanandan, L.-P. Lv, T. H. Tran, K. Landfester, D. Crespy, M. Rohwerder, *Adv. Mater.* **2013**, *25*, 6980.

14. M. F. Montemor, *Surf. Coat. Technol.* **2014**, *258*, 17.

15. R. Posner, N. Fink, G. Giza, G. Grundmeier, *Surf. Coat. Technol.* **2014**, *253*, 227 .

16. C. Fernández-Solis, A. Erbe, *Biointerphases* **2016**, *11*, 021001.

17. G. Grundmeier, M. Stratmann, *Annu. Rev. Mater. Res.* **2005**, *35*, 571.

18. N. S. Sangaj, V. C. Malshe, *Prog. Org. Coat.* **2004**, *50*, 28.

19. H. Haagen, W. Funke, *J. Oil Colour Chem. As.* **1975**, *58*, 359.

20. J. Comyn (Ed.), *Polymer Permeability*, Chapman & Hall, London **1985**.

21. R. J. Ashley, in J. Comyn (Ed.), *Polymer Permeability*, Chapman & Hall, London **1985**, 269–308.

22. D. Iqbal, R. S. Moirangthem, A. Bashir, A. Erbe, *Mater. Corros.* **2014**, *65*, 370.

23. P. Taheri, T. Wielant, T. Hauffman, J. R. Flores, F. Hannour, J. H. W. de Wit, J. M. C. Mol, H. Terryn, *Electrochim. Acta* **2011**, *56*, 1904.

24. P. Niehoff, P. Ebbinghaus, P. Keil, A. Erbe, *Appl. Surf. Sci.* **2012**, *258*, 3191.

25. A. Erbe, A. Sarfraz, C. Toparli, K. Schwenzfeier, F. Niu, in P. R. Lang, Y. Liu (Eds.), *Soft Matter at Aqueous Interfaces, Lect. Notes Phys.*, vol. 917, Springer, Cham, Switzerland, chap. 14 - Optical Absorption Spectroscopy at Interfaces **2016**, 459–490.

26. J. Brandrup, E. H. Immergut, E. A. Grulke, *Polymer Handbook, 4th Ed.*, Wiley, New York **1999**.

27. G. S. Frankel, M. Stratmann, M. Rohwerder, A. Michalik, B. Maier, J. Dora, M. Wicinski, *Corros. Sci.* **2007**, *49*, 2021.

28. W. Fürbeth, M. Stratmann, *Corros. Sci.* **2001**, *43*, 207.

29. M. Stern, A. L. Geary, *J. Electrochem. Soc.* **1957**, *104*, 56.

30. U. Bexell, M. Olsson, *Surf. Interface Anal.* **2001**, *31*, 223.

31. R. A. Nyquist, *Interpreting Infrared, Raman, and Nuclear Magnetic Resonance Spectra*, Academic Press, San Diego **2001**.

32. B. C. Trasferetti, C. U. Davanzo, M. A. Bica de Moraes, *J. Phys. Chem. B* **2003**, *107*, 10699.

33. D. Iqbal, A. Sarfraz, M. Stratmann, A. Erbe, *Chem. Commun.* **2015**, *51*, 16041.

34. P. Ebbinghaus, M. Rabe, A. Erbe, *Light, Energy and the Environment*, Optical Society of America, Washington, D.C., USA, **2016**, FTu2E.6, DOI: 10.1364/FTS.2016.FTu2E.6.

35. J. S. Mondragón Ochoa, A. Altin, A. Erbe, *Mater. Corros.* **2017**, *68*, 1326.

36. G. Frankel, D. Landolt, in A. Bard, M. Stratmann, G. Frankel (Eds.), *Encyclopedia of Electrochemistry*, vol. 4, Wiley-VCH, Weinheim, Germany, chap. 1.3 - Kinetics of Electrolytic Corrosion Reactions **2007**, 25–49.

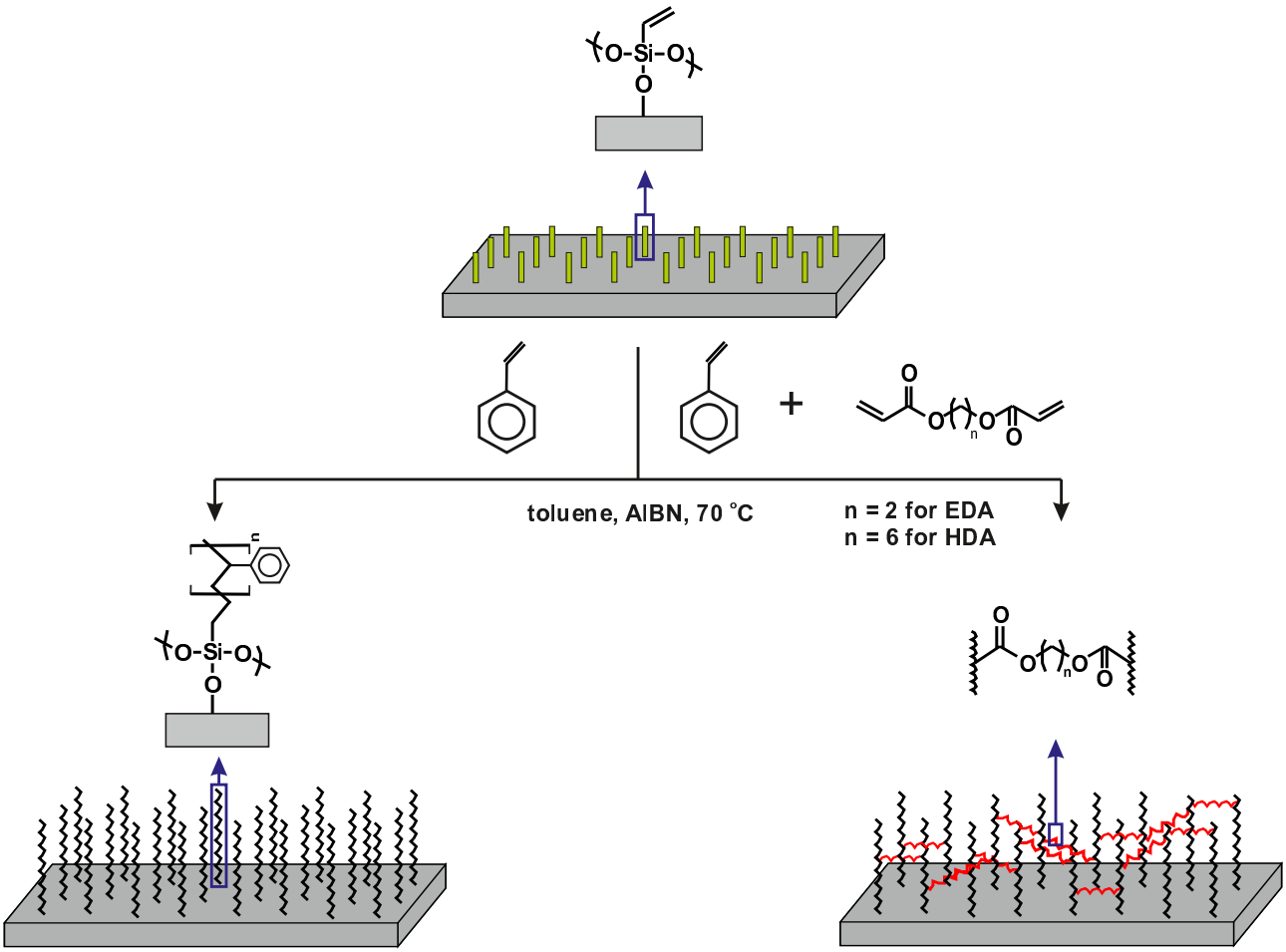


Figure 1: Schematic representation of the route for the synthesis of silane bonded linear and cross-linked PS coatings.

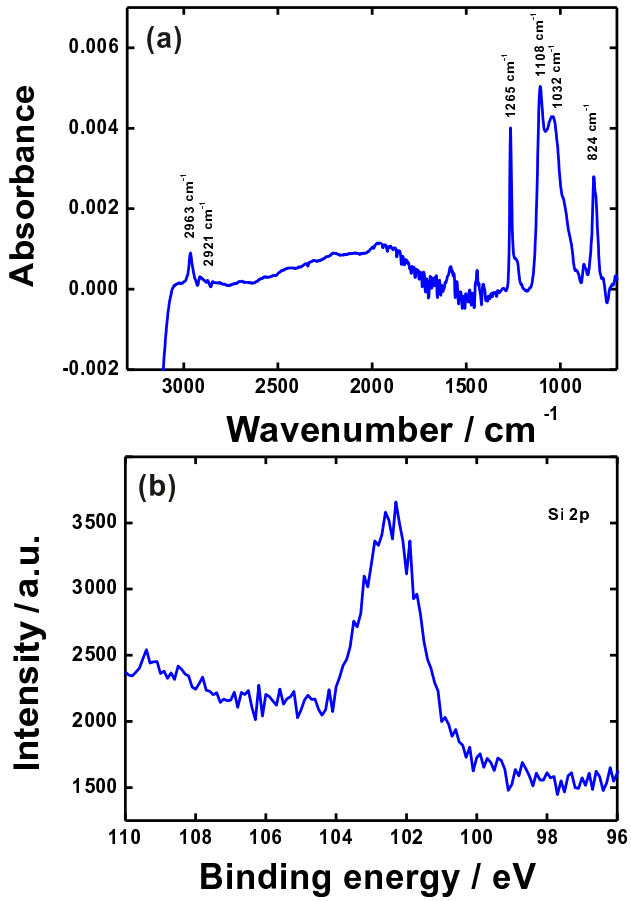


Figure 2: (a) IR spectrum of VTS-modified zinc. (b) Si 2p region of the XP spectrum of VTS-modified zinc. The presence of the signal confirms the presence of silane on the surface.

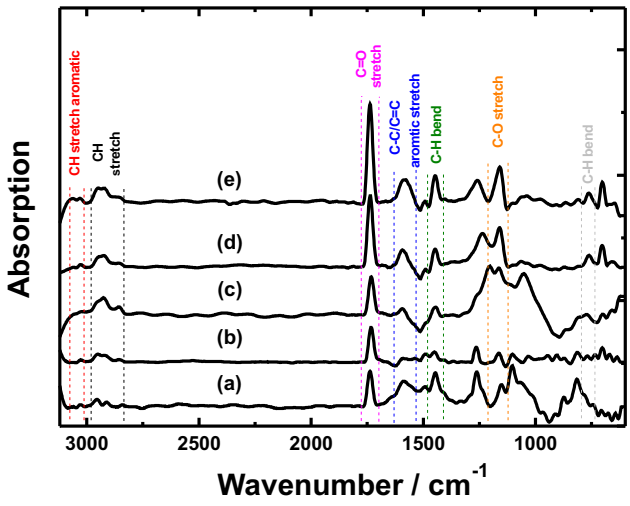


Figure 3: IR spectra of different covalently-bound polymer coatings on zinc. (a) PS without cross-linker, (b) PS + 25% EDA, (c) PS + 50% EDA, (d) PS + 25% HDA, (e) PS + 50% HDA. Empirical peak assignments are summarized in Table 1.

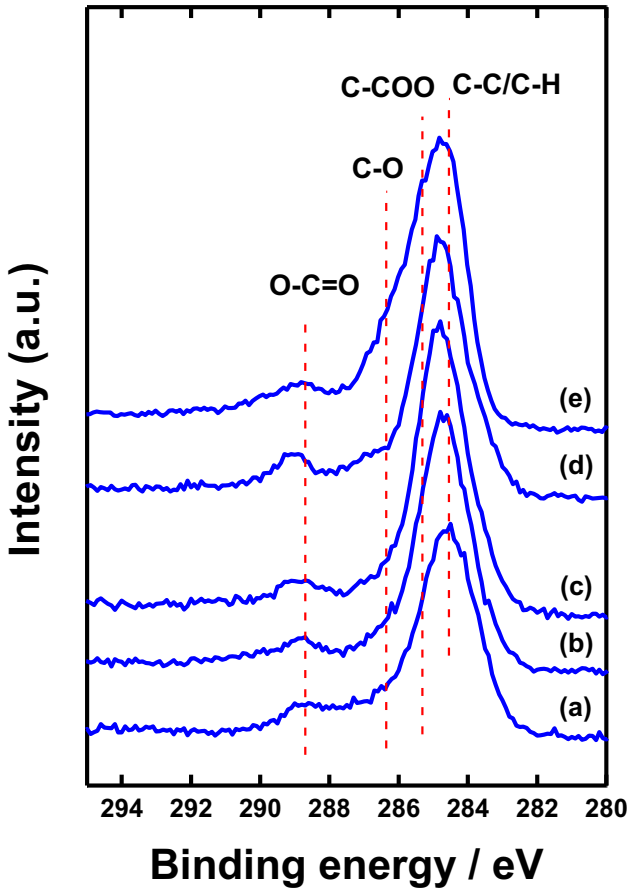


Figure 4: C 1s region of the XP spectrum of zinc with different polymer model coatings. (a) PS without cross-linker, (b) PS + 25% EDA, (c) PS + 50% EDA, (d) PS + 25% HDA, (e) PS + 50% HDA. The line represents the respective peak position for the molecule moiety shown in bold on its label.

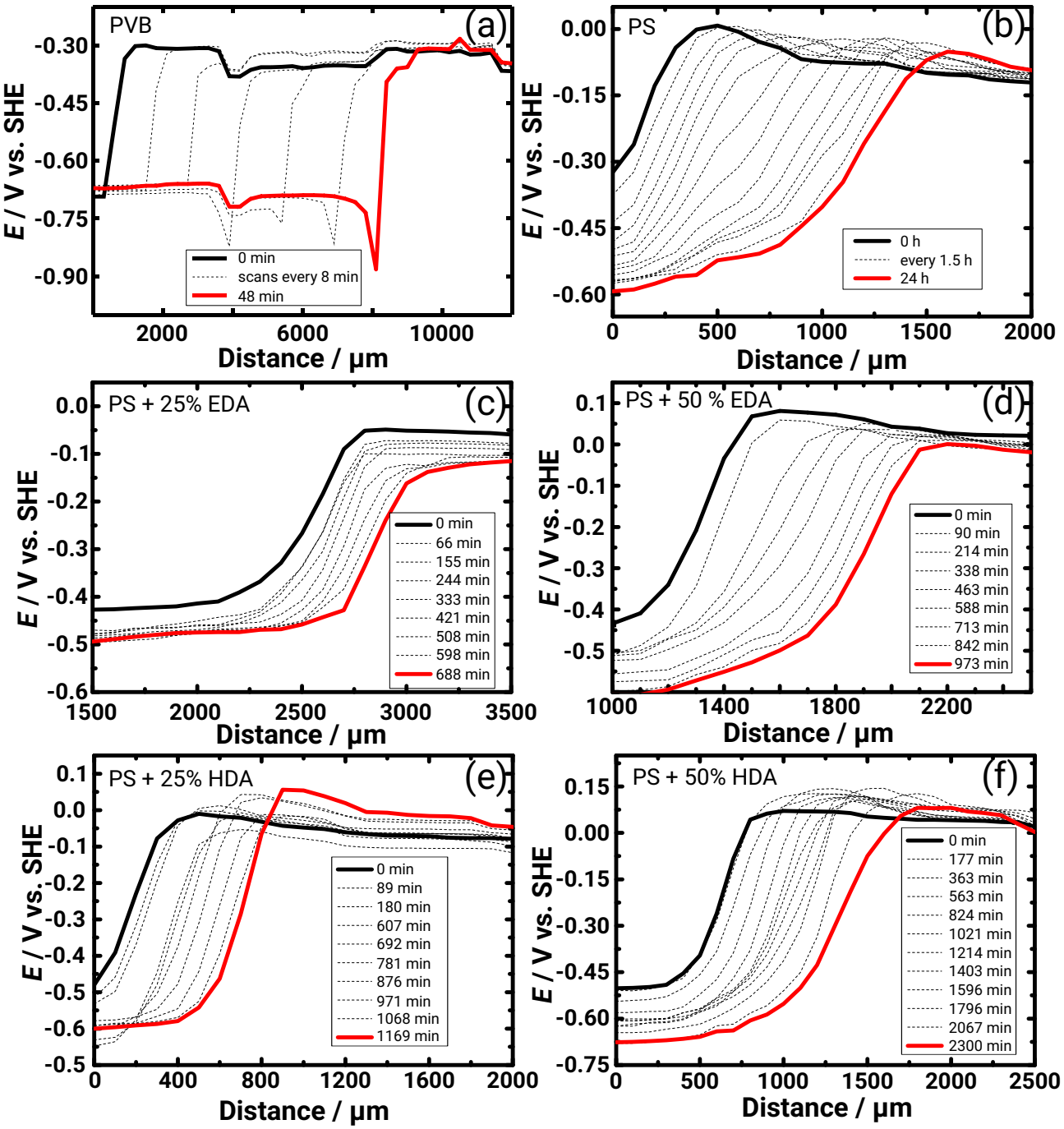


Figure 5: SKP potential profiles of (a) spin coated PVB on zinc, (b) covalently bound linear PS, (c) PS with 25% EDA, (d) PS with 50% EDA, (e) PS with 25% HDA, and (f) PS with 50% HDA. (b)-(f) include a PVB overcoat on zinc. The zero point on the length scale is arbitary.

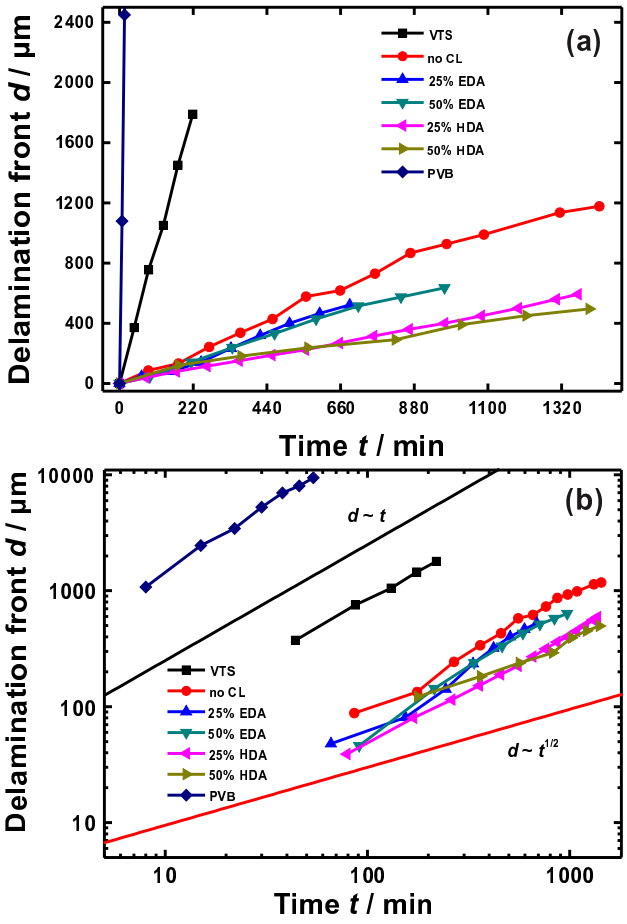


Figure 6: Progress of the position of the cathodic delamination front PVB-covered PS model coatings with different cross-linker amounts (a) on a linear scale and (b) on a double logarithmic scale. In plot (b), two lines show the expected slopes for $d \propto t$ and $d \propto t^{1/2}$, as indicated in the graph.

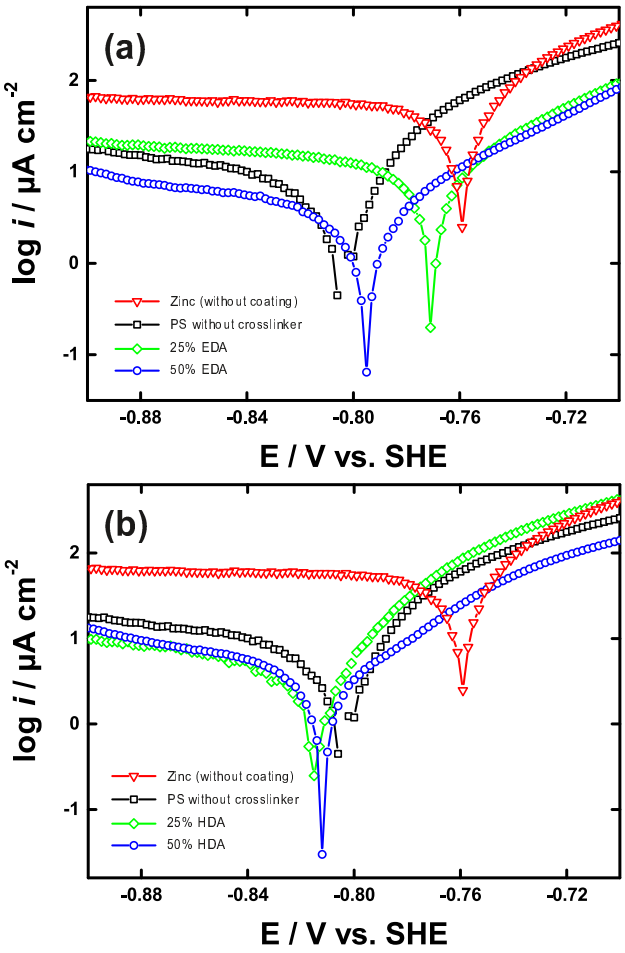


Figure 7: Tafel plots of bare zinc and PS covered zinc with different amounts of (a) EDA and (b) HDA.

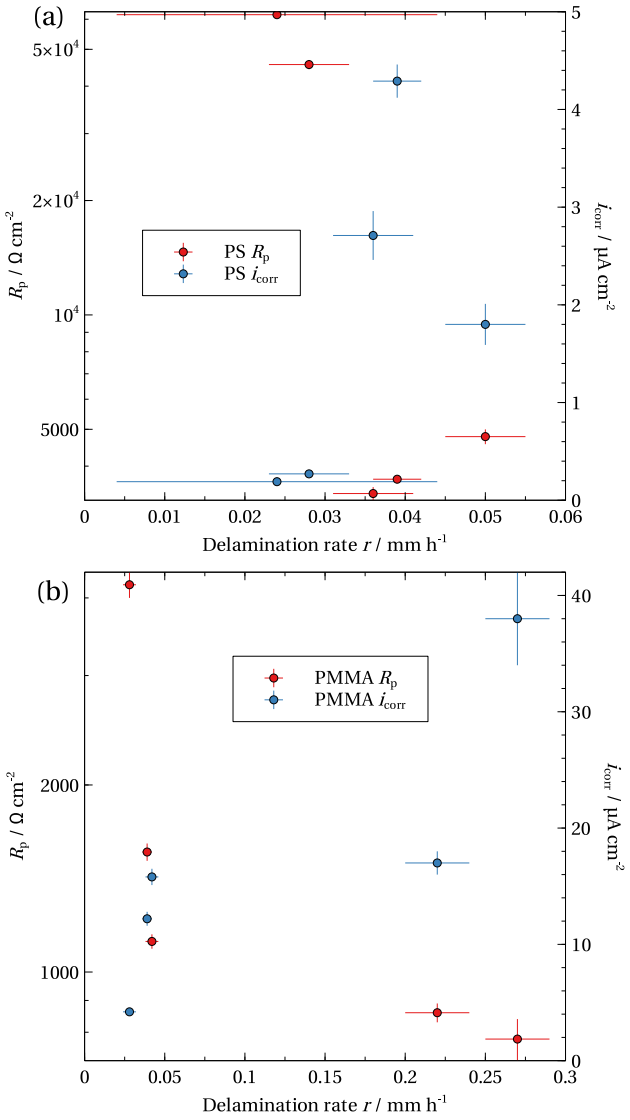


Figure 8: Plot of different parameters associated with interfacial stability against each other. Both $i_{\mathrm{corr}}$ and $R_{\mathrm{p}}$ are ploted versus the delamination rate $d$ of the same system; (a) data for the PS series discussed in this paper, and (b) data for a comparable series in PMMA published elsewhere.[7]

Table 1: IR peak positions, in $cm^{-1}$, of linear and cross-linked PS coatings synthesized on VTS-covered zinc surface and empirical assignments based on literature.[31] str.-stretching, sym.-symmetric, antisym.-antisymmetric.

| Peak assignment | PS | PS + 25% EDA | PS + 50% EDA | PS + 25% HDA | PS + 50% HDA |
|---|---|---|---|---|---|
| $C_{ar}$-$C_{ar}$ str. | 1589 | 1592 | 1579 | 1598 | 1594 |
| $C_{ar}$-$C_{ar}$ str. | 1494 | 1490 | 1492 | 1490 | 1444 |
| $C_{ar}$-H str. | 3060 | 3060 | 3058 | 3062 | 3056 |
| $CH_2$ antisym. str. | 2917 | 2922 | 2923 | 2922 | 2921 |
| $CH_2$ sym. str. | 2848 | 2848 | 2854 | 2851 | 2850 |
| $CH_2$ bend | 1446 | 1445 | 1446 | 1450 | 1444 |
| C=O str. | - | 1737 | 1737 | 1731 | 1731 |

Table 2: Thickness of synthesized linear and cross-linked PS coatings obtained from ellipsometric measurements, and cathodic delamination rate $d$ obtained from SKP measurements.

| Sample | Thickness [nm] | Delamination rate [mm $h^{-1}$] |
|---|---|---|
| PS | 15 ± 3 | 0.05 ± 0.005 |
| PS + 25% EDA | 10 ± 2 | 0.024 ± 0.02 |
| PS + 50% EDA | 8 ± 2 | 0.028 ± 0.005 |
| PS + 25% HDA | 8 ± 1 | 0.036 ± 0.005 |
| PS + 50% HDA | 10 ± 3 | 0.039 ± 0.003 |

Table 3: Corrosion current density $i_{corr}$, polarization resistance $R_p$ and anodic/cathodic Tafel slopes $\beta_a/\beta_c$ for the differently coated zinc samples in 0.1 M KCl.

| Sample | $\beta_a$ [mV dec$^{-1}$] | $\beta_c$ [mV dec$^{-1}$] | $R_p$ [Ω cm$^2$] | $i_{corr}$ [µA cm$^{-2}$] |
|---|---|---|---|---|
| zinc uncoated | 104 ±4 | 176 ±3 | 317 ±15 | 89 ±5 |
| PS | 33 ±1 | 49 ±6 | 4783 ±214 | 1.80 ±0.21 |
| PS + 25% EDA | 35 ±2 | 115 ±6 | 61679 ±1104 | 0.19 ±0.03 |
| PS + 50% EDA | 44 ±2 | 85 ±7 | 45593 ±1281 | 0.27 ±0.03 |
| PS + 25% HDA | 34 ±1 | 56 ±5 | 3388 ±135 | 2.71 ±0.25 |
| PS + 50% HDA | 50 ±0 | 136 ±3 | 3695 ±42 | 4.29 ±0.17 |

# Graphical abstract

Ultrathin, hydrophobic poly(styrene) model coatings have been prepared to investigate their cathodic delamination behaviour. The densly packed poly(styrene) delaminates slow, however, acrylate crosslinking increases the delamination rate.